AIP | Applied Physics Letters

Direct characterization of hydrodynamic loading on a microelectromechanical systems microstructure

Ali Mehrnezhad, Rashid Bashir, and Kidong Park

Citation: Applied Physics Letters **108**, 114101 (2016); doi: 10.1063/1.4944412
View online: http://dx.doi.org/10.1063/1.4944412
View Table of Contents: http://scitation.aip.org/content/aip/journal/apl/108/11?ver=pdfcov
Published by the AIP Publishing

Direct characterization of hydrodynamic loading on a microelectromechanical systems microstructure

Ali Mehrnezhad,[1] Rashid Bashir,[2,3] and Kidong Park[1,a)]
[1]*Division of Electrical and Computer Engineering, Louisiana State University, Baton Rouge, Louisiana 70803, USA*
[2]*Department of Bioengineering, University of Illinois at Urbana-Champaign, Urbana, Illinois 61801, USA*
[3]*Micro and Nanotechnology Laboratory, University of Illinois at Urbana-Champaign, Urbana, Illinois 61801, USA*

(Received 15 January 2016; accepted 4 March 2016; published online 16 March 2016)

Hydrodynamic loading greatly affects resonant characteristic of microfabricated structures immersed in a viscous fluid. In this letter, we demonstrate a technique to measure hydrodynamic loading on a MEMS resonator in a broad range of actuation frequency. The extracted hydrodynamic loading is in a good agreement with an analytical solution of an oscillating sphere, and a highly accurate model is developed for the hydrodynamic loading of the resonator. The developed technique can directly characterize the hydrodynamic loading of a microstructure with an arbitrary geometry and will facilitate the optimization of MEMS devices and AFM probes operating in a viscous fluid. © *2016 AIP Publishing LLC*. [http://dx.doi.org/10.1063/1.4944412]

Resonant characteristics of a microfabricated mechanical structure in a viscous fluid is one of the most important factors that determine the performances of various devices, including atomic force microscopy,[1–3] MEMS resonators,[4,5] and MEMS sensors.[6,7] When a microstructure is actuated in a viscous fluid, the surrounding fluid is moved by the microstructure, generating force that resists the movement. This resistive force is known as hydrodynamic loading and can be further divided into two factors, i.e., induced mass and viscous damping. The induced mass is the portion of the hydrodynamic loading which is linearly proportional to the acceleration of the microstructure. This is often referred to as "added mass,"[8,9] and it decreases the resonant frequency of the microstructure. Similarly, the viscous damping is the portion of the hydrodynamic loading, which is proportional to the microstructure's velocity.

Since the quality factor and the resonant frequency are major design parameters of microactuators, mechanical sensors, and resonators, there have been various research efforts to understand the hydrodynamic loading in a precise and quantitative manner. In an earlier literature,[10] the Navier-Stokes equation was solved for ideal geometries such as a sphere or a plane in order to understand the characteristics of the hydrodynamic loading. With increasing use of a microcantilever[7,11,12] as a mechanical structure for various MEMS devices, the hydrodynamic loading on the microcantilever has been actively investigated. Earlier, the cantilever was approximated by a sphere[13,14] to model the frequency response. Then, Sader *et al.* developed an analytic formula to estimate the quality factor and the hydrodynamic loading of a microcantilever with an arbitrary cross section.[1,15] Since then, various experimental studies were performed to characterize hydrodynamic loading and resulting changes in quality factor and resonant frequency.[15–18] Resonance of a microstructure immersed in a viscous fluid is often modeled as that of a second-order harmonic oscillator, and the hydrodynamic loading can be characterized using the resonant frequency and the quality factor extracted from the frequency response near the resonant condition. This approach can readily produce the induced mass and the viscous damping caused by the surrounding media. However, it is only applicable near the resonant frequencies and cannot characterize the hydrodynamic loading on a broad spectrum of the actuation frequency.

In this work, a technique that can directly characterize the hydrodynamic loading of a MEMS resonator in a broad range of actuation frequency is demonstrated. We also experimentally confirmed that the hydrodynamic loading has the same dependency to the actuation frequency as an analytical model of an oscillating sphere,[10] and developed a highly precise model of the hydrodynamic loading on our resonator.

The measurement setup is similar to our earlier studies and a MEMS mass sensor is used as a mechanical resonator.[19–21] The schematic diagram of the measurement setup is shown in Fig. 1. The resonator is immersed in a viscous liquid and it is actuated with Lorentz force by applying constant magnetic field in lateral direction and flowing actuation current perpendicular to the magnetic field. The velocity of the resonator is detected and characterized by a Laser Doppler Vibrometer (MSV-300, Polytec) and a lock-in-amplifier

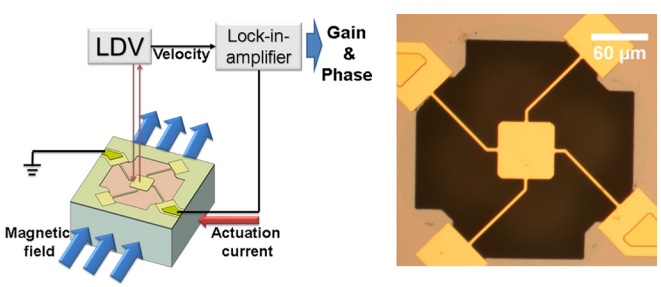

FIG. 1. (a) Experimental setup is shown. The structure immersed in a viscous fluid is actuated by Lorentz's force and its velocity is detected by LDV. The velocity signal from LDV is analyzed with a lock-in-amplifier. (b) Optical image of the resonator is presented.

[a)]Author to whom correspondence should be addressed. Electronic mail: kidongp@lsu.edu.

(Model 7280, Signal recovery). A typical resonant frequency of the resonator in deionized (DI) water is around 55 kHz and the amplitude is about 0.1 nm. The lock-in-amplifier provides the actuation current and also measures the amplitude and the phase of the measured velocity. The combination of the electromagnetic actuation, the Laser Doppler Vibrometer, and the lock-in-amplifier enables a highly linear and precise measurement of the frequency response.

The frequency responses of the same resonator in DI-water and glucose solutions are plotted in Figs. 2(a) and 2(b). In Fig. 2(a), the gain is defined as the ratio of the measured velocity to the applied Lorentz force. The phase presented in Fig. 2(b) is referenced to the actuation signal provided by the lock-in-amplifier, which is in sync with the Lorentz force. Since we are measuring the velocity rather than the displacement, the gain increases linearly as the actuation frequency increases and then decreases when the actuation frequency becomes larger than the resonant frequency. Also, the phase starts from $+90°$, becomes 0 at the resonant frequency, and then approaches $-90°$. DI water and glucose solutions with three different glucose concentrations (w/w), 9%, 18%, and 27%, are used in the measurement. The density of DI water and 9%, 18%, and 27% glucose solutions are 0.998 g/cm^3, 1.0340 g/cm^3, 1.0722 g/cm^3, and 1.113 g/cm^3, respectively.[22] The viscosity of DI water and 9%, 18%, and 27% glucose solutions are 0.890 cP, 1.294 cP, 1.790 cP, and 2.714 cP.[22] As expected, increasing concentration of glucose solution decreases the resonant frequency and the maximum gain. At the same time, the slope of the phase transition near the resonant frequency decreases as the concentration increases, indicating decreases in the quality factor. The resonant frequency and the quality factor are extracted from these measurements, as shown in Table I. The resonant frequency, f_0 is defined as the frequency where the velocity is in sync with the actuation force. The quality factor Q is defined as $Q = 0.5 \times \omega_0/(d\phi/d\omega)$, where ω_0, ϕ, and ω are the resonant angular velocity($\omega_0 = 2\pi f_0$), the phase, and the actuation angular velocity, respectively. The slope of the phase $d\phi/d\omega$ is evaluated at the resonant frequency.

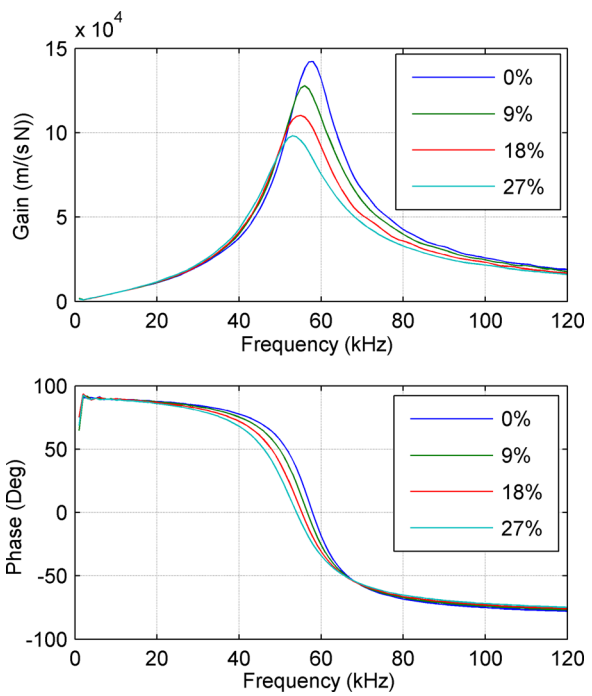

FIG. 2. Typical frequency responses of the velocity are presented. (a) Gain and (b) phase of the frequency responses in 4 different sample fluids, DI water (0%), 9%, 18%, and 27% glucose solutions, are shown.

In the following analysis, we assume that the resonator is made of hard materials, such as silicon, dielectric, and metal, which are commonly used in MEMS devices. Also, the resonator is assumed to be immersed in a viscous liquid. With these assumptions, structural damping or internal frictional loss of the resonator is much smaller than the viscous damping[1,23] caused by the hydrodynamic interaction and it is not considered in the analysis.

If we assume that the spring constant of the resonator in liquid is same as one in air, we can use the spring constant, k, measured in air, to calculate the induced mass, m, and the viscous damping, d in liquid near the resonant frequency, as follows:

$$m = \frac{1}{4\pi^2}\frac{k}{{f_0}^2} - m_{resonator}, \quad d = \frac{\sqrt{mk}}{Q}, \tag{1}$$

where $m_{resonator}$ is the mass of the resonator itself, which is 16.8 ng.[19] This approach is based on a second-order harmonic oscillator and can be used to approximate the behavior of the microstructure near the resonance condition. The spring constant, k, is calculated as $k = 4\pi^2\, m_{resonator}\, ({f_0}^{air})^2$, where ${f_0}^{air}$ is the resonant frequency of the resonator in air. The calculated value of k of five resonator used in this experiment is 12.883 ± 0.192 N/m. The induced mass and the damping calculated with Eq. (1) are listed in Table I.

It should be noted that the induced mass and the viscous damping extracted with the experimental approach in previous paragraph are valid only in the vicinity of the resonant frequency. Presently, to characterize the hydrodynamic loading with respect to the frequency, one should use analytical models and CFD (computational fluid dynamics) simulations, as demonstrated in earlier works.[1,2,24] Although such analytical and computational approaches can characterize the hydrodynamic loading without fabricating actual devices, there are still strong needs to directly measure the hydrodynamic loading of actual devices to accommodate the inherent variation in the fabrication process of the target devices and to experimentally validate analytical and computational models.

To directly measure the hydrodynamic loading on a broad range of the actuation frequency, the gain and the phase of the velocity at each actuation frequency can be used to extract the two unknowns, i.e., the induced mass and the viscous damping. The resonator is modeled as a second-order harmonic oscillator

$$F_{ext} = kX(j\omega) + j\omega dX(j\omega) + (j\omega)^2(m + m_{resonator})X(j\omega)$$
$$j\omega X(j\omega) = \frac{j\omega F_{ext}}{\left(k - (m + m_{resonator})\omega^2\right) + j\omega d}, \tag{2}$$

where F_{ext}, $j\omega X(j\omega)$, and $X(j\omega)$ are Lorentz force, velocity, and displacement of the resonator. The induced mass and the damping are assumed to be positive real numbers and

TABLE I. The induced mass and the viscous damping extracted from the resonant frequency and the quality factor based on a conventional approach as shown in Eq. (1) (n = 5).

	Resonant frequency (kHz)	Quality factor	Induced mass (ng)	Viscous damping (10^{-6} Ns/m)
DI water	58.304 ± 0.566	4.778 ± 0.018	79.219 ± 0.514	7.359 ± 0.028
9% Glucose solution	57.022 ± 0.570	4.291 ± 0.22	83.586 ± 0.590	8.380 ± 0.025
18% Glucose solution	55.648 ± 0.554	3.810 ± 0.025	88.604 ± 0.609	9.670 ± 0.055
27% Glucose solution	54.366 ± 0.547	3.415 ± 0.021	93.631 ± 0.658	11.044 ± 0.053

functions of density, viscosity, and actuation frequency. F_{ext} is assumed as a complex number and is in sync with the actuation current. Since the phase of the actuation current from the lock-in-amplifier is used as a reference phase, F_{ext}, is a positive real number too. Since the real part and the imaginary part of $j\omega X(j\omega)$ can be directly measured by the lock-in-amplifier, we can build following two equations to express m and d in terms of ω, k, real and imaginary parts of $j\omega X(jw)$[25]

$$m = \frac{1}{\omega^2}\left(k - 2\frac{\bar{C}^2\bar{D}}{\bar{C}^2+\bar{D}^2}\right) - m_{resonator}, \quad d = \frac{1}{\omega}\frac{2\bar{C}\bar{D}^2}{\bar{C}^2+\bar{D}^2}$$
$$\bar{C} = \frac{\omega}{2\mathrm{Re}[j\omega X(j\omega)]}, \quad \bar{D} = \frac{\omega}{2\mathrm{Im}[j\omega X(j\omega)]}. \tag{3}$$

Fig. 3 shows the induced mass and the viscous damping of the MEMS resonator. The resonator is immersed in DI water and 9%, 18%, and 27% glucose solutions. The average values of the induced mass and the viscous damping from 5 measurements with the frequency range of 40–120 kHz are shown as solid lines with error bars. With increasing concentration of the solution, we can see that the induced mass and the viscous damping increase accordingly. As shown in Fig. 3(a), the induced mass decreases as the actuation frequency increases. This can be explained by the decrease in the penetration depth with increasing actuation frequency. The penetration depth[10] δ is $\delta = (2\eta/\omega\rho)^{1/2}$, where η is a dynamic viscosity of the fluid. With increasing actuation frequency, the movement of the surrounding fluid attenuates quickly and the induced mass decreases. At the same time, the viscous damping increases with increasing frequency.

The measured result is compared to the analytical model of an oscillating sphere in an earlier literature.[10] In this model, a sphere immersed in a viscous fluid is oscillating vertically with a translational velocity, u. The hydrodynamic force acting on this sphere can be driven as follows:[10]

$$\begin{aligned} F &= 6\pi\eta R\left(1+\frac{R}{\delta}\right)u + 3\pi R^2\sqrt{\frac{2\eta\rho}{\omega}}\left(1+\frac{2R}{9\delta}\right)\frac{du}{dt} \\ &= \left(3\sqrt{2}\pi R^2\eta^{0.5}\rho^{0.5}\frac{1}{\sqrt{\omega}} + \pi R^3\frac{2}{3}\rho\right)\frac{du}{dt} \\ &\quad + \left(6\pi R\eta + 6\pi\frac{R^2}{\sqrt{2}}\eta^{0.5}\rho^{0.5}\sqrt{\omega}\right)u, \end{aligned} \tag{4}$$

where R and δ are the radius of the sphere and the penetration depth, respectively. We can separate the above force into two components, one correlated with the acceleration (du/dt) and the other correlated with the velocity (u). The former can be treated as the induced mass as it produces the

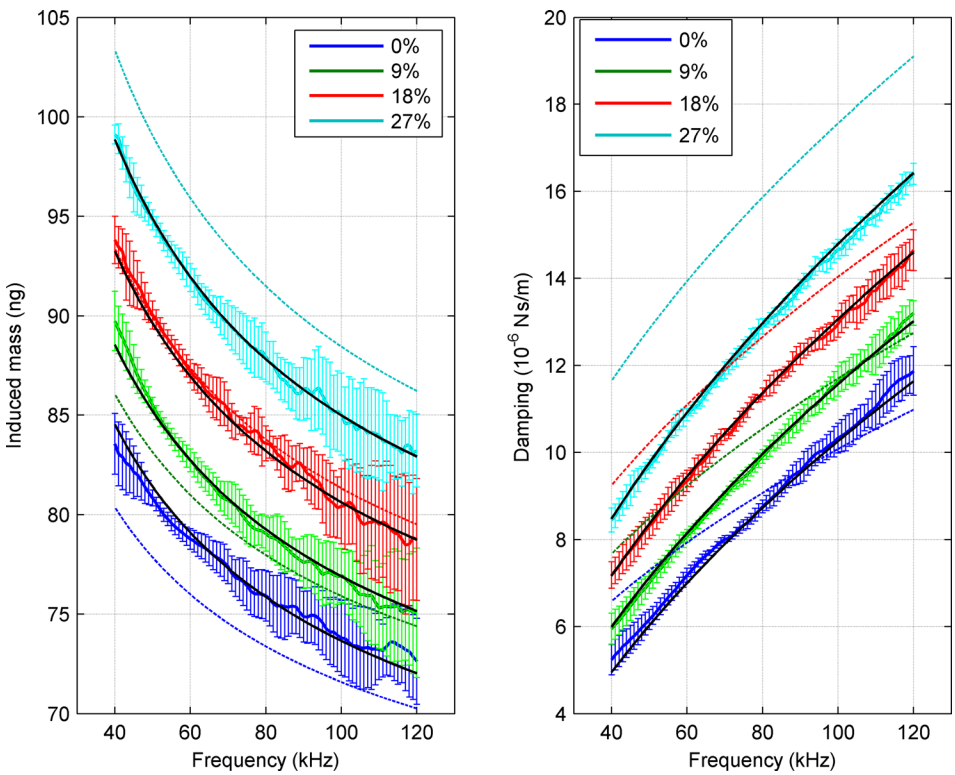

FIG. 3. The change of (a) the induced mass and (b) the damping on the resonator. The average values of the induced mass and the damping from 5 individual measurements are shown as a thick solid line. Standard deviations are shown with the error bars. The dashed lines are from the analytical model of the oscillating sphere with a radius of 30 μm. Black lines are from the fitted model.

force that is linearly proportional to the acceleration. The latter can be treated as the viscous damping as it is proportional to the velocity. The induced mass linearly increases as $\omega^{-0.5}$ increases. Also, the viscous damping increases linearly, as $\omega^{0.5}$ increases. Both of the induced mass and the viscous damping on the oscillating sphere in Eq. (4) are plotted in Fig. 3 as dashed lines. We set the radius of the sphere model, R to be 30 μm, as the center platform of the resonator is a $60 \times 60\ \mu m^2$. As shown in Fig. 3, both of the induced mass and the viscous damping of the MEMS resonator are similar to those of the oscillating sphere.

To further validate the similarity, the induced mass and the damping of the MEMS resonator are plotted against $\omega^{-0.5}$ and $\omega^{0.5}$. As can be clearly seen in Figs. 4(a) and 4(b), the induced mass and the damping are linear functions of $\omega^{-0.5}$ and $\omega^{0.5}$, respectively, preserving the characteristic of the oscillating sphere model in Eq. (4).

Although the extracted hydrodynamic loading of the MEMS resonator shows strong similarity to that of the oscillating sphere, it deviates from the analytic solution of the oscillating sphere. For instance, the induced mass of the resonator increased at a slower rate with increasing density and viscosity, comparing to the analytical model of the oscillating sphere. Also, the damping increased more rapidly than the analytical model, as the actuation frequency increases. We assumed that such deviation originates from the geometric difference between our resonator and the oscillating sphere.

To develop a precise model of the hydrodynamic loading on our resonator, the induced mass and the viscous damping of the resonator in DI water and glucose solutions were fitted into following equations:

$$\begin{aligned} m(\omega) &= p\frac{1}{\sqrt{\omega}} + q \\ d(\omega) &= r + s\sqrt{\omega}, \end{aligned} \tag{5}$$

where p, q, r, and s are fitting parameters. Table II shows these fitting parameters with each sample liquid. Then, we heuristically factored out density and viscosity from these fitting parameters, so that we can divide the fitting parameters into two factors, one that is dependent on the structure's geometry and the other that is dependent on the physical properties of the fluids, as shown in Eq. (6)

$$\begin{aligned} m(\omega) &= \bar{p} * \eta^{0.2}\rho^{0.5}\frac{1}{\sqrt{\omega}} + \bar{q} * \rho \\ d(\omega) &= \bar{r} * \eta^{-0.6} + \bar{s} * \eta^{0.125}\rho^{0.5}\sqrt{\omega}, \end{aligned} \tag{6}$$

where $\bar{p}$, $\bar{q}$, $\bar{r}$, and $\bar{s}$ are fitting parameters after factoring out the density and the viscosity. The means and standard deviations of $\bar{p}$, $\bar{q}$, $\bar{r}$, and $\bar{s}$ are $3.568 \times 10^{-9} \pm 0.318 \times 10^{-9}$, $3.907 \times 10^{-14} \pm 0.185 \times 10^{-14}$, $-6.663 \times 10^{-8} \pm 0.570 \times 10^{-8}$, and $1.369 \times 10^{-9} \pm 0.028 \times 10^{-9}$, respectively. The fitting parameters are presented in Table II. The fitted curves constructed by using the means of $\bar{p}$, $\bar{q}$, $\bar{r}$, and $\bar{s}$ extracted from four sample liquids are shown in Figs. 3(a) and 3(b) with black lines and show a strong agreement to the measured hydrodynamic loading. The maximum % error and the RMS % error of the induced mass are at most 1.82% and at most 0.80%, respectively.[25] The maximum % error and the RMS % error of the viscous damping are at most 5.54% and at most 1.99%, respectively. To further demonstrate the accuracy of the model in Eq. (6), we used $\bar{p}$, $\bar{q}$, $\bar{r}$, and $\bar{s}$ extracted from the experimental measurement of 9% glucose solution

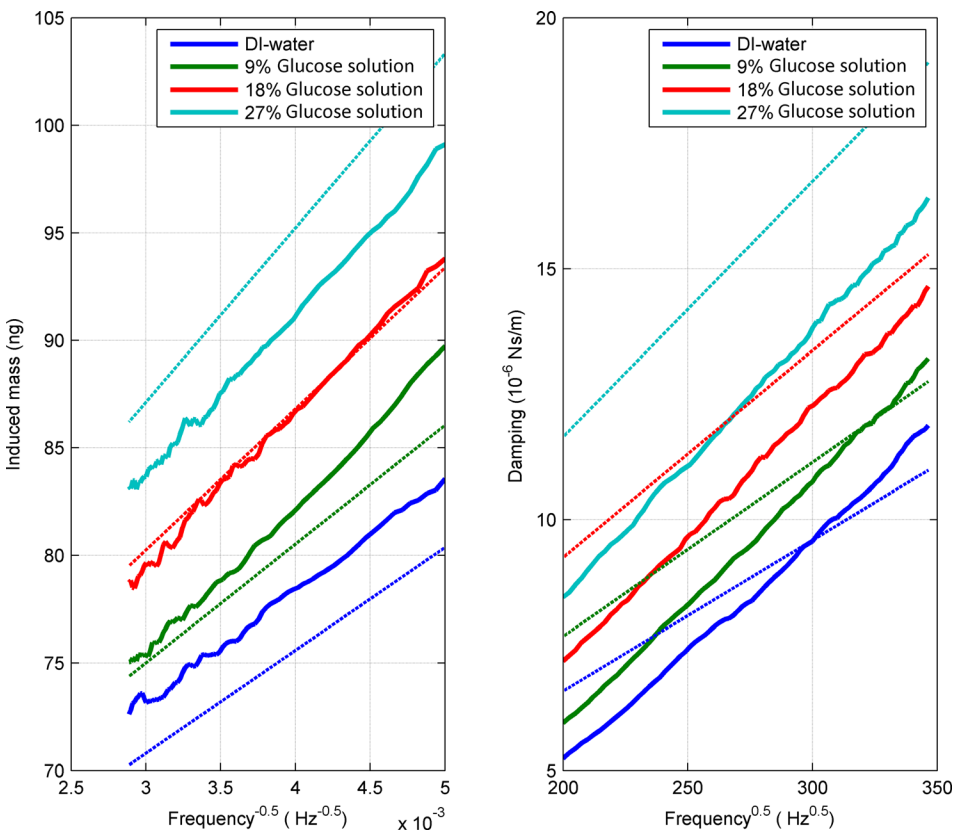

FIG. 4. The average values of (a) the induced mass and (b) the damping from 5 measurements are plotted with solid lines against $\omega^{-0.5}$ and $\omega^{0.5}$, respectively. The dashed lines are from the analytical model of the oscillating sphere with a radius of 30 μm.

TABLE II. The fitting parameters for Eqs. (5) and (6). The fitting parameters show less variation between each sample solutions after factoring out the density and the viscosity.

	p (10^{-7})	q (10^{-10})	r (10^{-5})	s (10^{-7})	$\bar{p}$ (10^{-8})	$\bar{q}$ (10^{-13})	$\bar{r}$ (10^{-7})	$\bar{s}$ (10^{-8})
DI water	0.129	0.410	−0.395	0.181	0.324	0.411	−0.627	0.136
9% glucose solution	0.172	0.381	−0.405	0.197	0.394	0.369	−0.747	0.141
18% glucose solution	0.181	0.410	−0.297	0.202	0.371	0.383	−0.660	0.136
27% glucose solution	0.188	0.444	−0.226	0.214	0.338	0.400	−0.632	0.135

and analyzed the error between the experimental data and the model. The maximum % error and the RMS % error of the induced mass are at most 3.28% and at most 1.75%, respectively. The maximum % error and the RMS % error of the viscous damping are at most 10.00% and at most 3.90%, respectively.[25] In spite of the large noise in the measurement data in Fig. 3, the model in Eq. (6) accurately predicts the experimental data.

In conclusion, the frequency response of a MEMS resonator in a viscous fluid is measured, and the hydrodynamic loading at a wide range of actuation frequency is directly characterized from the gain and phase of the velocity at each actuation frequency. The extracted hydrodynamic loading shows a good agreement with the analytical model of an oscillating sphere, and we clearly show that the induced mass and the viscous damping are linear functions of $\omega^{-0.5}$ and $\omega^{0.5}$, respectively. Furthermore, we developed a model for the hydrodynamic loading with a high precision and separated the fitting parameters of the model into a term dependent on the structure's geometry and a term dependent on the fluid's physical properties. We believe that the demonstrated technique would provide direct and precise characterization of the hydrodynamic loading on a microstructure with an arbitrary geometry and facilitate the optimization of various MEMS devices and AFM operating in a viscous fluid.

K. Park gratefully acknowledges support from the Louisiana Board of Regents (LEQSF(2014-17)-A-05) for this work.

[1]J. E. Sader, J. Appl. Phys. **84**(1), 64–76 (1998).
[2]S. Basak, A. Raman, and S. V. Garimella, J. Appl. Phys. **99**, 114906 (2006).
[3]H. Janovjak, J. Struckmeier, and D. J. Müller, Eur. Biophys. J. **34**(1), 91–96 (2005).
[4]J. Linden, A. Thyssen, and E. Oesterschulze, Appl. Phys. Lett. **104**(19), 191906 (2014).
[5]K. Eom, H. S. Park, D. S. Yoon, and T. Kwon, Phys. Rep. **503**(4), 115–163 (2011).
[6]K. Ekinci, Y. Yang, and M. Roukes, J. Appl. Phys. **95**(5), 2682–2689 (2004).
[7]B. N. Johnson and R. Mutharasan, Biosens. Bioelectron. **32**(1), 1–18 (2012).
[8]Y. Lee, G. Lim, and W. Moon, Microsyst. Technol. **13**(5–6), 563–567 (2007).
[9]J. Kongthon, B. McKay, D. Iamratanakul, K. Oh, J.-H. Chung, J. Riley, and S. Devasia, J. Vib. Acoust. **132**(2), 024501 (2010).
[10]L. D. Landau and E. M. Lifshitz, *Fluid Mechanics* (Addison-Wesley, Reading, Massachusetts, 1959).
[11]K. M. Hansen and T. Thundat, Methods **37**(1), 57–64 (2005).
[12]P. S. Waggoner and H. G. Craighead, Lab Chip **7**(10), 1238–1255 (2007).
[13]H. J. Butt, P. Siedle, K. Seifert, K. Fendler, T. Seeger, E. Bamberg, A. Weisenhorn, K. Goldie, and A. Engel, J. Microsc. **169**(1), 75–84 (1993).
[14]G. Chen, R. Warmack, T. Thundat, D. Allison, and A. Huang, Rev. Sci. Instrum. **65**(8), 2532–2537 (1994).
[15]J. W. M. Chon, P. Mulvaney, and J. E. Sader, J. Appl. Phys. **87**, 3978 (2000).
[16]K. Yum, Z. Wang, A. P. Suryavanshi, and M.-F. Yu, J. Appl. Phys. **96**(7), 3933–3938 (2004).
[17]C. Vančura, I. Dufour, S. M. Heinrich, F. Josse, and A. Hierlemann, Sens. Actuators, A **141**(1), 43–51 (2008).
[18]I. Dufour, E. Lemaire, B. Caillard, H. Debéda, C. Lucat, S. M. Heinrich, F. Josse, and O. Brand, Sens. Actuators, B **192**, 664–672 (2014).
[19]K. Park, N. Kim, D. T. Morisette, N. Aluru, and R. Bashir, J. Microelectromech. Syst. **21**(3), 702–711 (2012).
[20]K. Park, L. J. Millet, N. Kim, H. Li, X. Jin, G. Popescu, N. Aluru, K. J. Hsia, and R. Bashir, Proc. Natl. Acad. Sci. U. S. A. **107**(48), 20691–20696 (2010).
[21]K. Park, J. Shim, V. Solovyeva, E. Corbin, S. Banerjee, and R. Bashir, Appl. Phys. Lett. **100**(15), 154107 (2012).
[22]W. M. Hanes, Handbook of Chemistry and Physics (CRC, Boulder, Colorado, 2011).
[23]C. A. Van Eysden and J. E. Sader, J. Appl. Phys. **101**(4), 044908 (2007).
[24]C. P. Green and J. E. Sader, J. Appl. Phys. **92**(10), 6262–6274 (2002).
[25]See supplementary material at http://dx.doi.org/10.1063/1.4944412 for details.